



# Growth and characterization of TiAlN nanoparticles using low-energy plasma focus device

Hasan Anousha<sup>1</sup> · Eslam Gharehabani<sup>1</sup>

Received: 10 May 2019 / Accepted: 11 July 2019 / Published online: 27 July 2019  
© The Author(s) 2019

## Abstract

In this experimental study, a 1.5-kJ plasma focus device of Mather type was employed to grow titanium aluminum nitride (TiAlN) coatings at room temperature on 316 stainless steel sub-layer. The anode of the device was made of Titanium and Aluminium. A mixture of N<sub>2</sub> and Ar gases was used as the work gas for TiAlN deposition. TiAlN nanoparticles were formed on stainless steel with 0° of the degree with respect to the anode axis by different shots at 5 cm above the anode. X-ray diffraction results indicated the formation of the TiAlN structure on stainless steel. Scanning electron microscopy images demonstrated the approximately uniform growth of TiAlN nanoparticles on the surface. EDX analysis results showed that an increase in the number of the shots increased the deposition of TiAlN on the sub-layer. According to the atomic force microscopy images, the mean thickness of the surface increased as the shots increased in number. Microhardness test results of the thin layers showed that an increase in the number of the shots increased the hardness of the samples.

**Keywords** TiAlN · Plasma focus · Nanoparticles · XRD · SEM

## Introduction

Titanium aluminum nitride (TiAlN) is a refractory and very hard material. Due to its physical and chemical properties, from high-temperature resistance to corrosion resistance, it is widely used for coating in high-temperature technologies [1]. TiAlN consists of titanium and aluminum and has the following advantages over titanium nitride:

(1) Oxidation resistance at high temperatures (800–900 °C) due to the formation of the protective aluminum oxide layer; (2) higher hardness (3000 HV); and (3) lower electrical and thermal conductivity [1–3].

TiAlN coatings have wurtzite structure at a high-Al portion over Ti, while they are in the form of B1-NaCl at a high-Ti portion over Al (Fig. 1).

TiAlN nanoparticles have been deposited by different methods among which are physical vapor deposition (PVD) [4–6], sputtering [7, 8], chemical vapor deposition (CVD) [9], and laser/sol–gel method [10]. TiAlN nanoparticles have

also been formed by other plasma focus devices with different energies and configurations [11, 12].

In this study, the plasma focus device of Tabriz Sahand University of Technology was employed to grow TiAlN nanoparticles on stainless steel sub-layer. The nanoparticles were formed on the stainless steel with different numbers of shots. The synthesized samples were examined for their structure by XRD, in surface morphology by SEM, in elements dispersion on the sub-layer by mapping analysis, in topography and surface thickness by AFM, and in grown elements combination on the sub-layer by EDX.

## Methodology

A Mather-type plasma focus device of Tabriz Sahand University of Technology consisted of a copper anode electrode with 1.8 cm of diameter and 5.3 cm of length, surrounded by six bronze cathode electrodes, each with 5.3 cm of length. A Pyrex insulator has separated the electrodes (Fig. 2). In this experiment, the anode was made of Ti and Al. There was a shutter between the anode electrode and the sample holder for the initial shots to achieve an excellent pinch. The entire set of the electrodes was placed inside a vacuum container that was pressure-dropped by a rotary compressor to 0.2 torr.

✉ Hasan Anousha  
hassan.anoosha@yahoo.com

<sup>1</sup> Department of Physics, Faculty of Basic Sciences, Sahand University of Technology, Tabriz, Iran

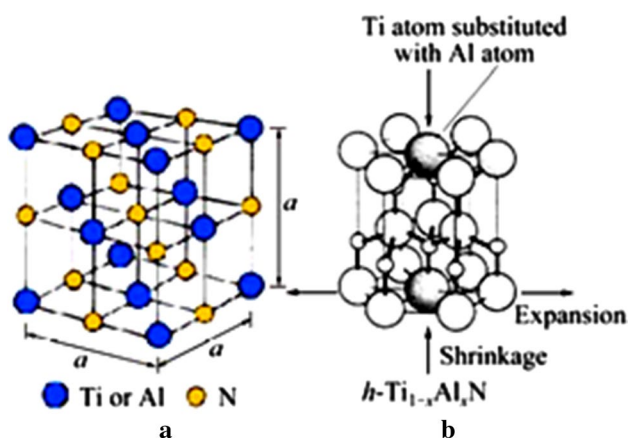


Fig. 1 TiAlN lattice structure for a B1-NaCl and b wurtzite

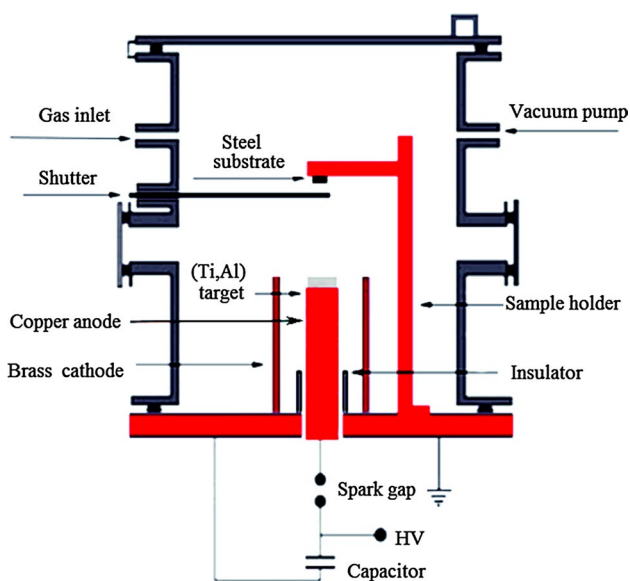


Fig. 2 Schematic of Mather-type plasma focus device

Then, a mixture of  $N_2$  and Ar gases was injected inside the vacuum container as the working gas.

The optimum pressure for the excellent pinch in the experiment was 0.2 torr at 6 kV of voltage. The voltage wave form versus current at pinch time, which was received from Rogowski coil, was recorded by an oscilloscope (Fig. 3).

For the operation of the plasma focus device, a high voltage was applied between two anode and cathode electrodes by three 10  $\mu$ F capacitors charged by a high voltage. Then, an electrical discharge took place on the insulator surface in 100 ns, creating a current layer on the insulator surface. A self-consistent magnetic field is created, producing Lorentz force and accelerating the current layer to the open end of the anode. As a result, the  $J \times B$  force compressed the current layer on the anode, which created

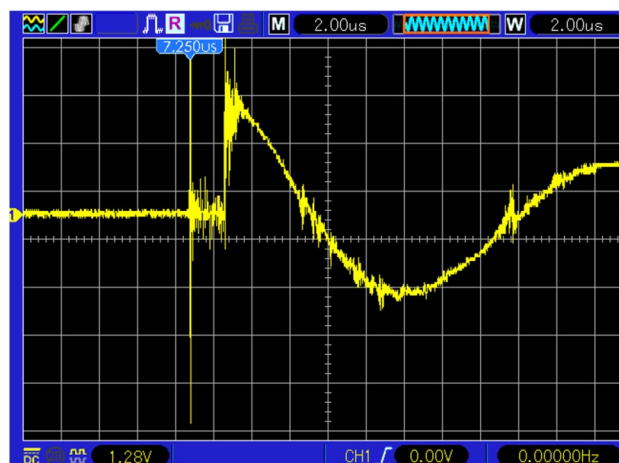


Fig. 3 Rogowski coil current derivative signal at pinch time

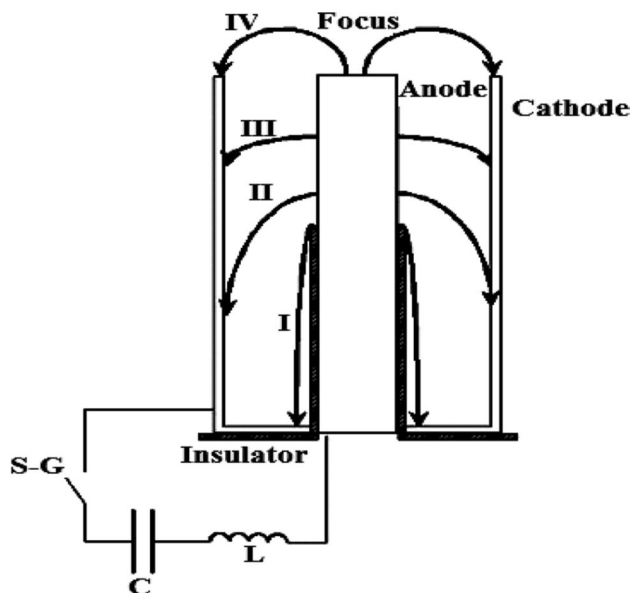
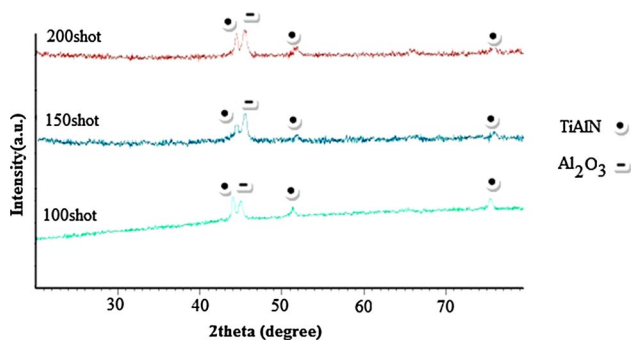


Fig. 4 Dynamics of the plasma focus device

warm dense plasma. At this time, the plasma column created by the sausage instability ( $m=0$ ) was eliminated by the production of high-energy electron, ion, and X-ray particles. Since a strong magnetic field was created when the plasma column was eliminated, this magnetic field accelerated the ions and electrons in opposite directions such that the high-energy electrons collided with the anode (Ti, Al) and resulted in their melt. Ti and Al atoms were mixed with the ionized  $N_2$  gas and deposited on the sub-layer at the pinch time by the produced plasma jet (Fig. 4). Before the formation of the nanoparticles, steel samples were cleaned with alcohol, acetone, and distilled water, each for 20 min in an ultrasonic device with the help of ultrasonic waves.



**Fig. 5** X-ray diffraction spectrum for the samples synthesized with **a** 100 shots, **b** 150 shots, and **c** 200 shots

The samples were placed 5 cm above the anode. (Ti, Al) N nanoparticles were also placed at  $0^\circ$  with respect to the anode axis with 100, 150, and 200 shots, being analyzed by XRD, SEM, AFM, EDX, and mapping devices.

### X-ray spectroscopy results

The XRD spectroscopy of the samples was done using a grazing technique which is specific to thin layers and coatings. Figure 5 represents the X-ray diffraction spectrum of the synthesized samples with different shots. The diffraction spectrum shows the formation of the TiAlN crystalline phase for the samples grown on steel. Different peaks of TiAlN crystalline planes were observed at  $2\theta$  of  $44.3^\circ$ ,  $51.9^\circ$ , and  $75.6^\circ$  along with  $\text{Al}_2\text{O}_3$  at  $45.7^\circ$ . The diffraction peak locations are matched with the standard data for TiAlN. Hence, the patterns indicate the growth of TiAlN crystals on steel.

The average size of TiAlN was measured by Scherrer's formula in Eq. 1, where  $\lambda$  is a wavelength of Cu  $K\alpha$  radiation 0.154 nm,  $D$  is the size of the crystal,  $\beta$  is FWHM, and  $K$  is the Scherrer constant, which in this case was 0.9. From this formula, the average particle size of 100, 150 and 200 shots is 47, 52 and 100 nm, respectively

$$d = \frac{0.9\lambda}{\beta \cos \theta} \quad (1)$$

### SEM results

Figure 6 demonstrates the SEM images for TiAlN nanoparticles on the steel sub-layer. These particles are almost uniformly distributed on the surface. As it is observed, the increased number of the shots increased the deposition on the sub-layer, with the particles starting to join together. The size of the nanoparticles has been increased at 200 shots,

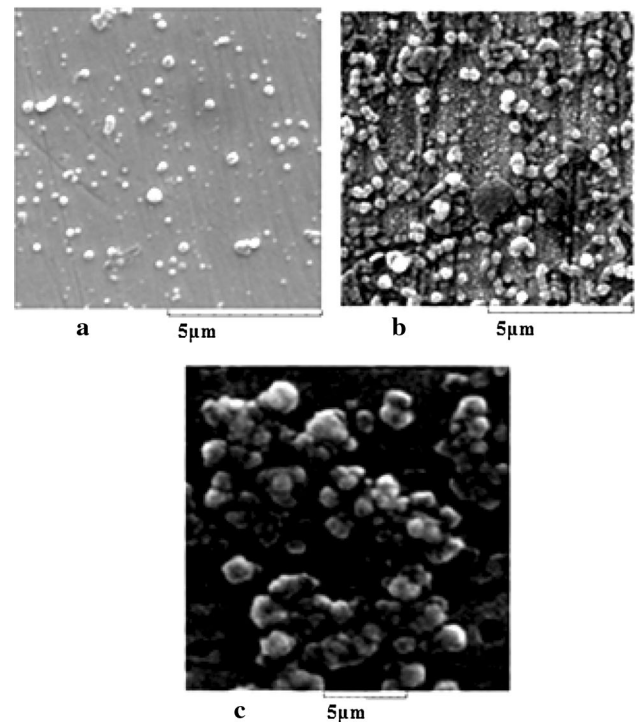


**Fig. 6** SEM images at **a** 100 shots, **b** 150 shots, **c** 200 shots

which can be attributed to the increased surface energy due to the increased shot number and deposition.

### AFM results

To measure roughness of the surface of the samples, a microscope of atomic force is used in noncontact state. The AFM images show that the number of the shots is increased from 100 to 200 and the nanoparticles size is increased from  $40 \pm 10$  nm to  $90 \pm 10$  nm which is corresponded with the XRD results. The mean surface thickness was 188 nm at 100 shots, which was increased to 359 nm as the number of the shots increased to 200. This can be due to the increased energy of the ions passed toward the sub-layer (Fig. 7).

### EDX results

EDX analysis was employed to identify the elements constituting the samples. Figure 8 shows the weight percentage graph of the elements grown on the sub-layer at different numbers of shots. EDX results indicate that an increase in the number of the shots affects TiAlN grown on the sub-layer—i.e., it increases TiAlN deposition. At 100 shots, a high content of TiAlN atoms does not have sufficient energy to reach the sub-layer and grow on it due to their

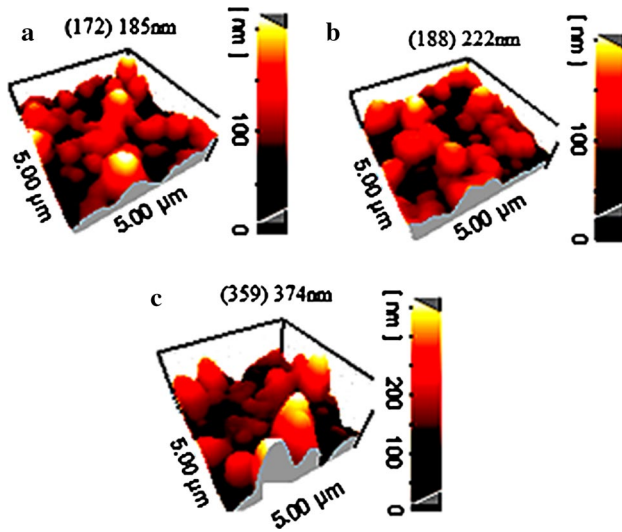


**Fig. 7** AFM images for the nanoparticles grown at **a** 100 shots, **b** 150 shots, and **c** 200 shots

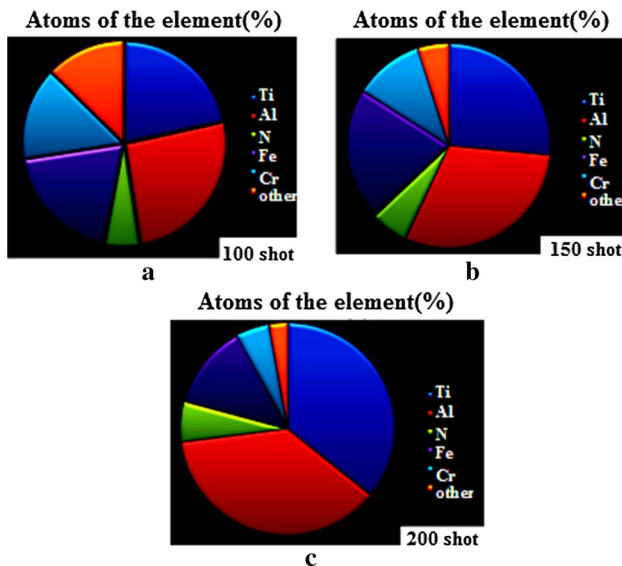


**Fig. 8** Atomic weight graph of the elements deposited on the sub-layer at **a** 100, **b** 150, and **c** 200 shots

high weights and low velocities. Another reason is that the atoms separated from the anode surface are conically dispersed when the focus collapses and the number of TiAlN atoms getting vertically close to the sub-layer is decreased.

## Mapping results

This analysis was performed to measure the uniformity of the thin layer and investigate the dispersion of the elements on the sub-layer by SEM, in which the locations of the deposited

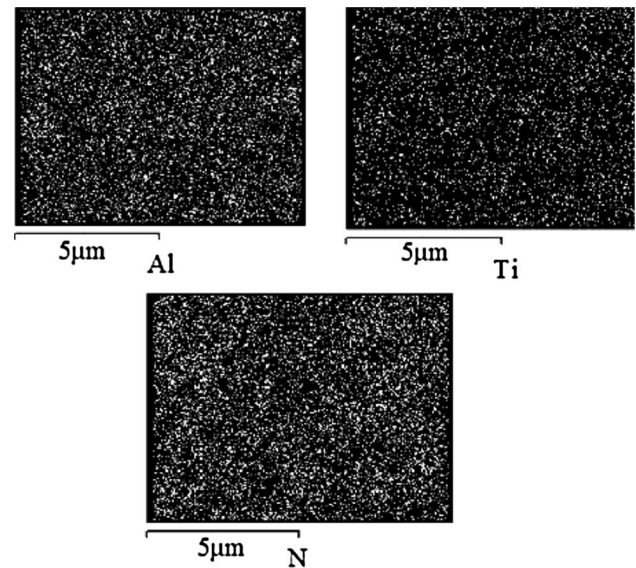


**Fig. 9** Layer elements dispersion

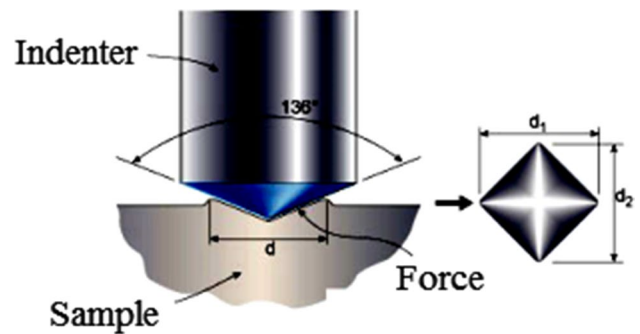


**Fig. 10** Schematic of Vickers hardness

atoms on the sub-layer are indicated by the device. Figure 9 represents Ti, Al, and N atoms on the steel sub-layer. Mapping results show TiAlN deposition as uniform on the sub-layer.

## Microhardness results

Microhardness is a mechanical property of thin layers, which relates to tensile strength. In this method, a square pyramid penetrator with  $136^\circ$  of apex angle is used. The penetrator penetrates in the sample surface with a given force and makes a rectangular sign with the diameters of  $d_1$  and  $d_2$  (Fig. 10). Vickers hardness number (DPH) is calculated as force/penetrated area. The penetrated area is calculated from microscopic lengths and diameters. Thus, we have

$$\text{DPH} = \frac{2P \sin\left(\frac{\theta}{2}\right)}{L^2} = \frac{1.854P}{L^2} \quad (2)$$

where  $P$  is the force in kg,  $L$  is the mean length of the diameters in mm, and  $\theta$  is the pyramid apex angle (i.e.,  $136^\circ$ ). Given the microhardness results, the hardness of the samples deposited at 100, 150, and 200 shots was 243, 260, and 286 VH, respectively.

## Conclusion

1. TiAlN nanoparticles were grown on 316 stainless steel sub-layer using a 1.5-kJ Mather-type plasma focus device.
2. XRD results indicated the formation of TiAlN structure on the sample surfaces, which is matched with the standard data for TiAlN.
3. According to SEM images and EDX analysis, an increase in the number of the shots resulted in a higher deposition on the sub-layer, increasing the size of the nanoparticles.
4. According to AFM images, the mean surface thickness is increased as the shots increase in number.
5. According to the microhardness results, the increased number of the shots increased the hardness of the deposited samples from 243 to 286 VH.

**Author contributions** HA is responsible author and carried out the experiment and EG is supervisor and project support.

**Open Access** This article is distributed under the terms of the Creative Commons Attribution 4.0 International License (<http://creativecommons.org/licenses/by/4.0/>), which permits unrestricted use, distribution, and reproduction in any medium, provided you give appropriate credit to the original author(s) and the source, provide a link to the Creative Commons license, and indicate if changes were made.

## References

1. Liu, G.T., Duh, J.G., Chung, K.H., Wang, J.H.: Mechanical characteristics and corrosion behavior of (Ti, Al)N coatings on dental alloys. *Surf. Coat. Technol.* **200**(7), 2100–2105 (2005)

2. Munz, W.D.: Titanium aluminum nitride films: a new alternative to TiN coatings. *J. Vac. Sci. Technol.* **4**(6), 2717–2725 (1986)
3. Tousif, H., Riaz, A., Jamil, S., Nida, Kh.: TiAlN coatings synthesized using a dense plasma focus system and varied focus shots. *Radiat. Eff. Defects Solids* **166**(11), 873–883 (2011)
4. Chawla, V., Chawla, A., Mehta, Y., Puri, D., Prakash, S., Sidhu, B.S.: Investigation of properties and corrosion behaviour of hard TiAlN and AlCrN PVD thin coatings in the 3 wt% NaCl solution. *J. Aust. Ceram. Soc.* **47**(1), 48–55 (2011)
5. Ahlgren, M., Blomqvist, H.: Influence of bias variation on residual stress and texture in TiAlN PVD coatings. *Surf. Coat. Technol.* **200**, 157–160 (2005)
6. Kim, G., Lee, S., Hahn, J.: Properties of TiAlN coatings synthesized by closed-field unbalanced magnetron sputtering. *Surf. Coat. Technol.* **193**, 213–218 (2005)
7. Shum, P.W., Li, K.Y., Zhou, Z.F., Shen, Y.G.: Structural and mechanical properties of titanium–aluminium–nitride films deposited by reactive close-field unbalanced magnetron sputtering. *Surf. Coat. Technol.* **185**, 245–253 (2004)
8. Quesada, F., Marino, A., Restrepo, E.: TiAlN coatings deposited by r.f. magnetron sputtering on previously treated ASTM A36 steel. *Surf. Coat. Technol.* **201**, 2925–2929 (2006)
9. Das, S., Guha, S., Ghadai, R., Kumar, D., Swain, B.P.: Morphological and structural properties of CVD deposited titanium aluminium nitride (TiAlN) thin films. In: *IOP Conference Series: Materials Science and Engineering*, vol. 377 (2018). <https://doi.org/10.1088/1757-899x/377/1/012178>
10. Sundar, M., Kamara, A.M., Mativenga, P.T., Li, L.: Synthesis of TiAlN based coating on mild steel substrate using combined laser/sol-gel technique. *Surf. Coat. Technol.* **204**, 2539–2545 (2010)
11. Hosseinejad, M.T., Ghorannevis, Z., Soltanveisi, M., Shirazi, M.: Preparation of titanium carbide thin film using plasma focus device. *J. Fus. Energy* **516**, 30 (2011)
12. Hussain, T., Ahmad, R., Khalid, N., Umar, Z.A., Hussain, A.: Synthesis of nanostructured multiphase (Ti,Al)N/a-Si<sub>3</sub>N<sub>4</sub> thin films using dense plasma focus device. *Nucl. Instrum. Methods Phys. Res. B* **269**, 1951–1955 (2011)

**Publisher's Note** Springer Nature remains neutral with regard to jurisdictional claims in published maps and institutional affiliations.